ENTE PER LE NUOVE TECNOLOGIE,
L'ENERGIA E L'AMBIENTE

ISSN/0393-3016

ϒ IRRADIATION FACILITY AT ENEA-CASACCIA CENTRE (ROME)

S. BACCARO, A. CECILIA, A. PASQUALI

ENEA - Unità Tecnico Scientifica Tecnologie Fisiche Avanzate
Centro Ricerche Casaccia, Roma

RT/2005/28/FIS

ENTE PER LE NUOVE TECNOLOGIE,
L'ENERGIA E L'AMBIENTE

ϒ IRRADIATION FACILITY AT ENEA-CASACCIA CENTRE (ROME)

S. BACCARO, A. CECILIA, A. PASQUALI

ENEA - Unità Tecnico Scientifica Tecnologie Fisiche Avanzate
Centro Ricerche Casaccia, Roma

RT/2005/28/FIS

IMPIANTO DI IRRAGGIAMENTO γ CALLIOPE PRESSO IL CENTRE RICERCHE ENEA-CASACCIA (ROMA)

Riassunto

In questo lavoro viene descritto l'impianto di irraggiamento γ "Calliope" del Centro Ricerche ENEA-Casaccia (Roma). In particolare vengono riportate le principali caratteristiche dell'impianto di irraggiamento necessarie per definire le modalità di tempo e di irraggiamento. Le tecniche dosimetriche utilizzate sono: la dosimetria di Fricke, la Red-Perspex e quella ESR con alanina. Nel primo caso la dose assorbita è misurata attraverso cambiamenti chimici indotti dalla radiazione in una soluzione mentre nel secondo metodo si utilizza l'aumento della densità ottica del dosimetro dovuto all'irraggiamento. Infine la tecnica ESR ad alanina si basa sull'analisi dei radicali liberi indotti dall'irraggiamento nell'aminoacido α-alanina.

Nel lavoro è anche fornita una simulazione del campo di radiazione all'interno della cella di irraggiamento realizzata con il codice FLUKA, che include un'ottima descrizione dei processi di iterazione elettromagnetici fino ad un'energia di 1\,keV.

Parole chiave: radiazione γ, Dosimetria, Impianto di irraggiamento.

γ IRRADIATION FACILITY AT ENEA-CASACCIA CENTRE (ROME)

Abstract

A description of "Calliope" γ irradiation plant of ENEA-Casaccia Centre (Rome) is presented in this paper. In particular the main characteristics of the irradiation facility necessary to define time and irradiation procedure are summarised. The plant is equipped with dosimetric services that evaluate absorbed doses in materials during irradiation. Dosimetric techniques used are Fricke, Red-Perspex and alanine-ESR dosimetries. In the first case, absorbed dose is determined by chemical changes induced in a solution by irradiation and the second method uses the optical density increase induced in dosimeter by irradiation. The last method is based on the analysis of the free radical concentration induced in α-alanine amino-acid during irradiation.

The paper provides also a simulation of the γ radiation field inside the irradiation cell realised by using FLUKA code, which includes a good description of the electromagnetic physics down to about 1\,keV.

Keywords: γ radiation, Dosimetry, Irradiation plant.

Index

Introduction

The aim of this work is the description of "Calliope" γ irradiation plant (Research Centre ENEA-Casaccia, Rome) and the definition of the physical sizes, methods, devices and/or set-ups used to measure absorbed dose in inorganic, organic, organic-biological and/or devices submitted to γ irradiation.

The term *ionising radiation* refers to each kind of radiation able to induce ionisation and/or excitation of atoms through primary and secondary interactions, when radiation impinges matter.
Charged particles induce ionisation and excitation processes through *Coulombic* interaction with atomic electrons. Generally, X- and γ-rays interact with matter through three main processes: photoelectric effect, Compton scattering and pair production. The result of that interaction is the emission of secondary charged particles, which in turn may induce further ionisation and excitation processes.
Neutron too may induce the production of secondary charged particles through different kinds of interaction, such as *(n, p)*, *(n, d)*, *(n, α)* or *(n, t)* processes; in this sense they can be considered ionising radiation.
Other kinds of radiation, such as UV, can not be considered ionising due to their inability to cross the greatest part of materials [1, 2].

According to ASTM E 170-76 [3], dosimetry is the process through which it is possible to obtain measurements describing an ionisation, a radiation field, some of the field components or the absorption in matter of the field associated energy.

Dosimeter techniques can be divided in *"absolute"* and *"relative"* methods: in the first case, they allow the absorbed dose estimation by the measurement of a physical size; an example is represented by the absolute calorimetric dosimetry, based on the temperature increase of the irradiated medium. On the contrary, relative dosimeters require an inter-calibration with an absolute method [4]. At Calliope plant three kinds of dosimeters are used: *Fricke* solution, *Red Perspex* and *alanine* dosimeter. Among them, the solid state dosimeter methods (*Red Perspex* and *alanine*) are *relative* measurement methods and they are periodically calibrated with an absolute dosimeter method, which is represented by Fricke dosimeter.

At present, the plant is involved in radiation processing research on industrial materials, such as polymers and on devices to be used in hostile radiation environment such as nuclear plants, aerospace experiments and High Energy Physics experiments [5-30]. As it will be shown in paragraph 2.2, very special cares are devoted to the qualification of electronic devices, which have to be tested according to either MIL-STD-883 and ESA/SCC BASIC Specifications No.22900 procedures.

Chapter 1: Calliope irradiation plant and dosimetry

1.1 Irradiation plant

The Calliope plant, located at the Research Centre ENEA-Casaccia, was constructed in 1967-68 to carry out research activities and pilot experiences on agricultural product treatment by radiation (seed stimulation and food irradiation). Differently, in the eighties the plant has been involved in radiation processing research on industrial materials (polymers and optical fibres) and on devices to be used in hostile radiation environment such as nuclear plants, aerospace experiments and High Energy Physics experiments. One of the main activities carried out in the Laboratory of the Calliope plant concerns the R&D of scintillating materials to be used as detectors in High Energy and Medium Energy Physics experiment.

The Calliope plant is a pool-type irradiation facility equipped with a ^{60}Co γ source [31, 32] in a high volume (7×6×3.9 m^3) shielded cell. The source has cylindrical geometry with the 48 source rods arranged in two concentric cylinders of about 20 cm outer radius and 26 cm height (Figure 1).

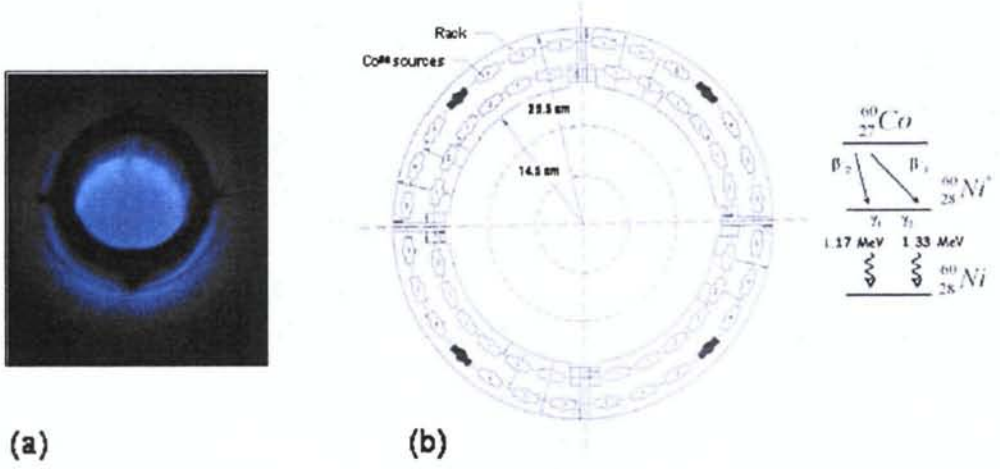

Figure 1: *Cherenkov* effect[1] (a) and top view of the Calliope facility with ^{60}Co decay (b)

The emitted radiation consists of two γ photons of 1.173 and 1.332 MeV emitted in coincidence, with a mean photon's energy of 1.25 MeV. The maximum licensed activity for this plant is 3.7×10^{15} Bq (100 kCi) but the present activity is 6.72×10^{14} Bq (18.1 kCi) at January 2005 the 1st. In this plant it is possible to choice the dose rate at which to irradiate the sample. 5.4 kGy/h is the maximum dose rate along the rack longitudinal axis. The storage water pool dimensions are 2×4.5×8 m^3 and two separate source emergency storage wells are positioned on the bottom of the pool. On the roof of the cell a trap door allows the introduction or the withdraw of radioactive materials in case of source recharge. The irradiation cell biological protection is realised in baritic concrete having thickness up to 180 cm. The main Calliope features are reported in Table I; moreover, Figure 2 and 3 reports the lateral and x-y view of the plant. Inside the irradiation cell, a humidity measuring element ("Polyga TM", AMPERE S.p.A.) is positioned for the measurement of relative air humidity, temperature and ozone which are recorded by a coupled Data-Chart 2000 Series (Ampere S.p.A.). The system detector & recorder is particularly useful in case of sudden scream, because it allows to date the exact time of the scream. Moreover, the possibility to transfer acquired data on PC by a flash card allows the emission of an official irradiation certificate.

[1] *Cherenkov* radiation is electromagnetic radiation emitted when a charged particle passes through an insulator at a speed greater than that of light in the medium. The characteristic "blue glow" of nuclear reactors is due to *Cherenkov* radiation. It is named for P. A. Cherenkov, the 1958 Nobel Prize winner who was the first to rigorously characterize it.

Table I: Calliope main features

SOURCE:	^{60}Co, SS double encapsulated;
GEOMETRY:	cylindrical rack, with radioisotope pencils placed on two levels of external rack surface;
EMITTED RADIATION:	2 γ photos emitted in coincidence;
PHOTON ENERGY:	1.173 and 1.332 MeV (average 1.25 MeV);
MAX LICENSED ACTIVITY:	3.7×10^{15} Bq (100 kCi);
PRESENT ACTIVITY(1-2-05) :	6.72×10^{14} Bq (18.1 kCi);
MAX DOSE RATE:	5.4 kGy/h along the rack longitudinal axis.

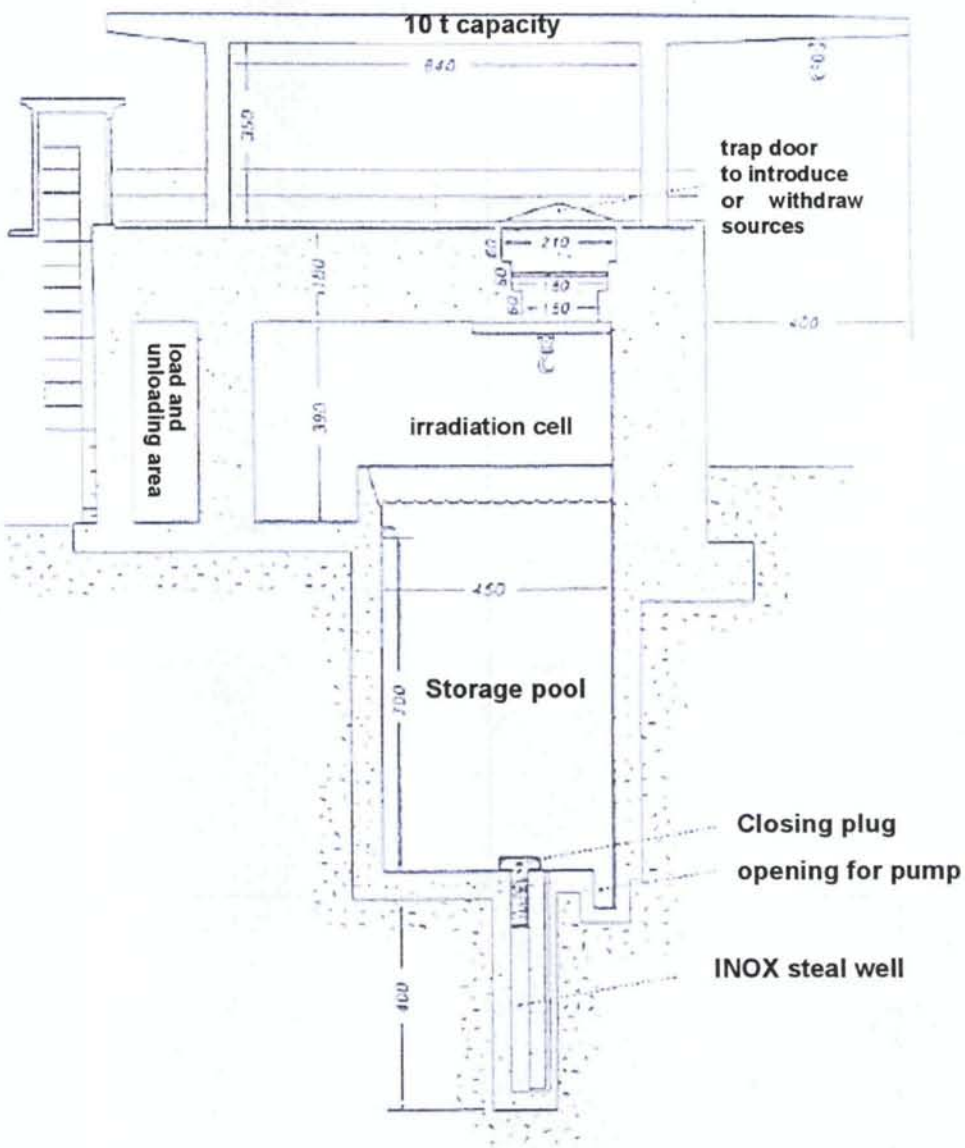

Figure 2: Lateral view of the Co^{60} plant

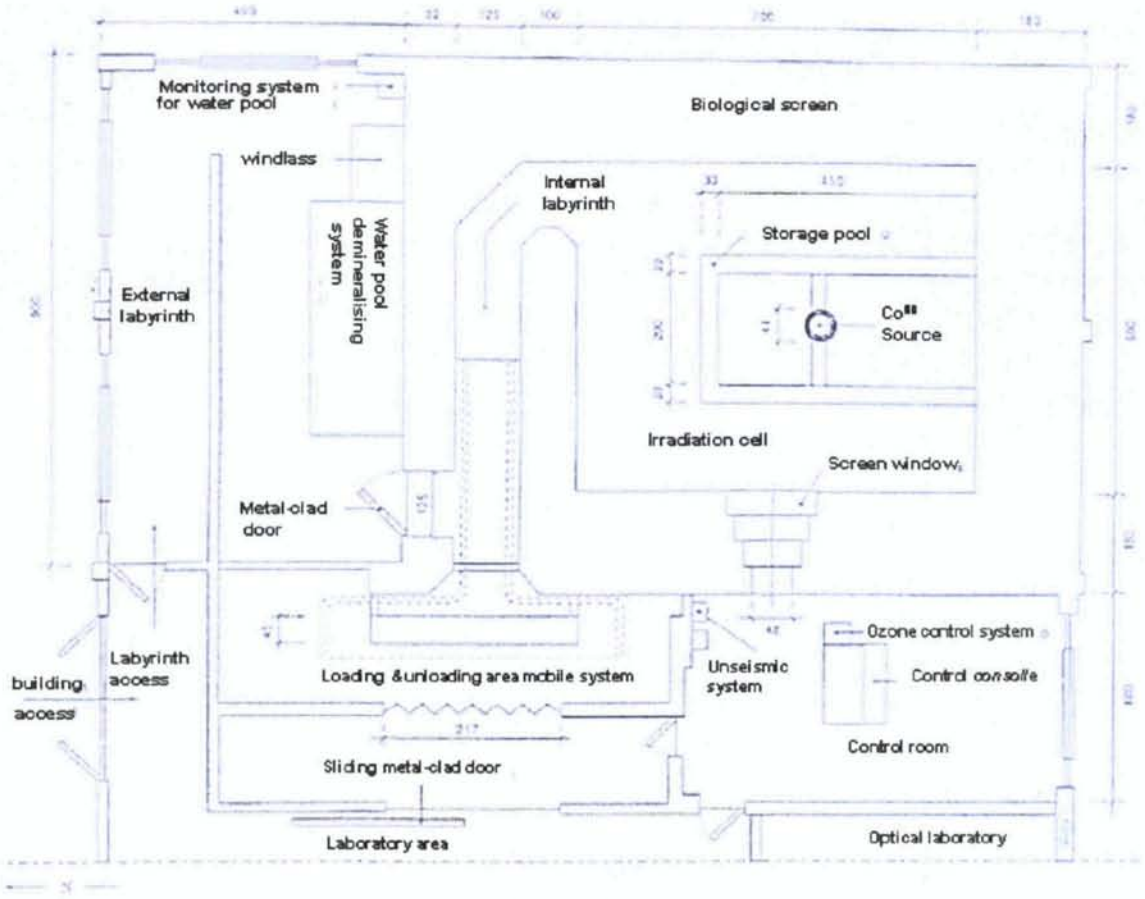

Figure 3: Calliope plant x-y view

Recently, we have carried out some modifications in the irradiation cell, thanks to which materials can be irradiated in isodose positions surrounding the source rack: a steel platform was projected and realised, covering the pool and characterised by a central circular aperture for the passage of the source (Figure 4).

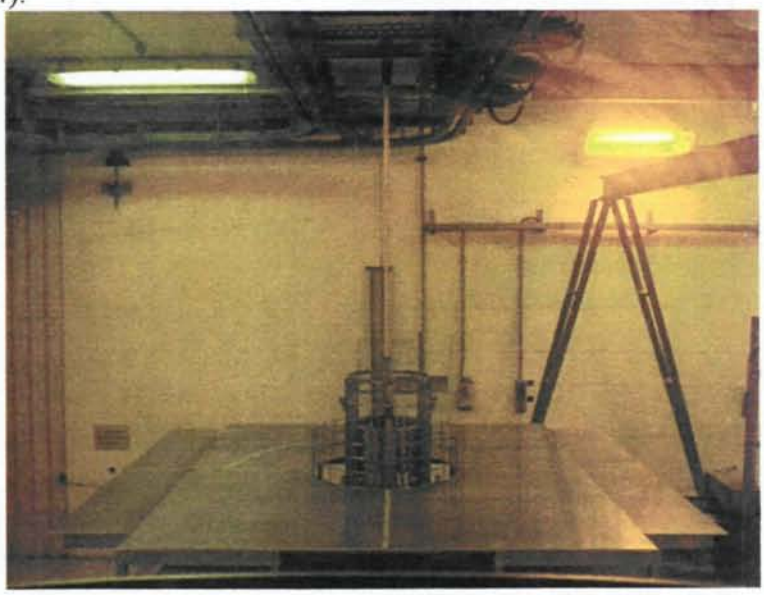

Figure 4: Realised steel platform covering the pool photographed through the yellow lead window of the Control Room.

That platform is equipped with movable arc measurers individuating the isodose positions on the platform and provided with compartments for the housing of dosimeters. As shown in detail in Figure 5, each measurer is composed of two parallel steel arcs that can be vertically moved. Such property makes possible to investigate horizontal and vertical dose rate uniformity, which are fundamental information for samples under irradiation. This equipment can be also used to host object to irradiate.

Figure 5: Detail of arc measurers

In addition to devices useful on the platform described above, we also projected and realised 4 steel movable mountings, shown in Figure 6, which can be moved in different dosimetric positions of the irradiation cell and which allow the repeatable sample positioning. It is also possible to put more supports on the same tree to irradiate few samples at the same dose rate: in any case it is important to verify that homogeneity of dose rate on the maximum surface involved in the irradiation test.

Figure 6: Movable mountings

1.2 Irradiation and dosimetry

A radiation generates in its surroundings a radiation field including either directly or indirectly ionising radiation. In the first case, radiation consists of charged particles having sufficient energy to produce ionisation and/or excitation via collision processes; in the second case radiation consists of uncharged particles (photons, neutrons, etc.) whose interaction with matter gives rise either to directly ionising particles or nuclear reactions.

Dosimetry is the process through which it is possible to obtain a measurement describing an ionisation, a radiation field, some field components or the absorption in the matter of the field associated energy. The most used size in radiation dosimetry, furnishing a quantitative correlation between radiation and its effect, is the absorbed dose.

According to ICRU-Report 33 [33], the absorbed dose is defined as the ratio between energy ($d\varepsilon$) released from radiation to matter in a certain volume and the volume mass (dm):

$$D = \frac{d\varepsilon}{dm} \tag{1}$$

In (1) ε is the energy released in the volume from an ionising radiation field, defined as:

$$\varepsilon = R_{in} - R_{out} + \sum Q \tag{2}$$

where:

- R_{in} is the radiant energy entering the volume V, or sum of the energies (with the exception of the rest energy) of all directly and indirectly ionising particles entering the considered volume;
- R_{out} is the radiant energy leaving the volume V, or the sum of the energies (with the exception of the rest energy) of all directly and indirectly ionising particles going out from the considered volume;
- $\sum Q$ is sum of all released energies minus the sum of all the energy expended in each nuclear transformation and in the elementary processes happened in the volume V.

In the SI the absorbed dose is measured in Gray (Gy) equivalent to 100 rad:

$$1\ Gy = 1\ \frac{J}{Kg} \tag{3}$$

The dose rate is the dose absorbed per unit time:

$$\dot{D} = \frac{dD}{dt} \tag{4}$$

1.2.1 Charge particle equilibrium and thickness

Let us consider a volume V_1 of air in which a uniform photon radiation field is present (Figure 7). Moreover, in the internal part of V_1 let us take into consideration a small volume V_2 whose distance from V_1 is high enough to brake secondary electron radiation. Due to the interaction with matter, in the volume V_2 photons will give rise to secondary electrons which will be meanly equal (in energy and number) to electrons produced in every V_2 volume. The consequence is that the number of electrons entering a volume V_2 with a certain energy and direction will be equal to the number of electrons having the same properties and leaving the same volume. That condition is known as the *charge particle equilibrium condition* and it guarantees no storage of secondary electrons in every volume V_2, because the energy lost out of every volume V_2 is equal to the energy lost in V_2 by secondary particles produced outside each volume [1, 34].

To realize the charged particle equilibrium conditions during an irradiation, irradiated sample should be surrounded by an absorber of suitable thickness, defined as the *charged particle equilibrium thickness*. The thickness value depends on sample electron density and on the energy of impinging radiation. In the curve representing the absorbed dose dependence on sample depth (Figure 8) that value corresponds to the thickness where the curve achieves its highest value. As it can be seen, the curve is characterised by an initial increasing course due to fluency increment of

the electrons coming from foregoing layer. Next, as the depth increases, photon attenuation causes an electronic fluence decrease and consequently a decrease of absorbed dose.

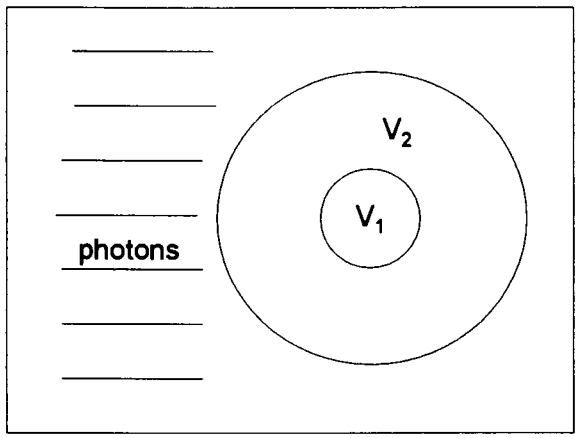

Figure 7: Air volumes immersed in an uniform photon radiation field

The equivalent thickness of a certain material can be obtained by the following relation:

$$S_{eq} = \frac{n_{H_2O}}{n_x} \cdot S_{H_2O} \qquad (5)$$

where n_{H_2O} is the water electronic density, S_{H_2O} is the electronic equilibrium thickness for water [35] and n_x is the electronic density of the material, defined as:

$$n_x = \rho \frac{N_A}{M} \sum_i Z_i \qquad (6)$$

where:
- ρ is the material density [Kg m^{-3}];
- N_A is the Avogadro number [$6.023*10^{23}$ $moli^{-1}$];
- M is the molecular mass [Kg $moli^{-1}$];
- Z_i is the atomic number of the i-material;
- ΣZ_i is the total number of electron per molecule.

Figure 9 reports the dependence of the water electronic equilibrium thickness on the photon energy.

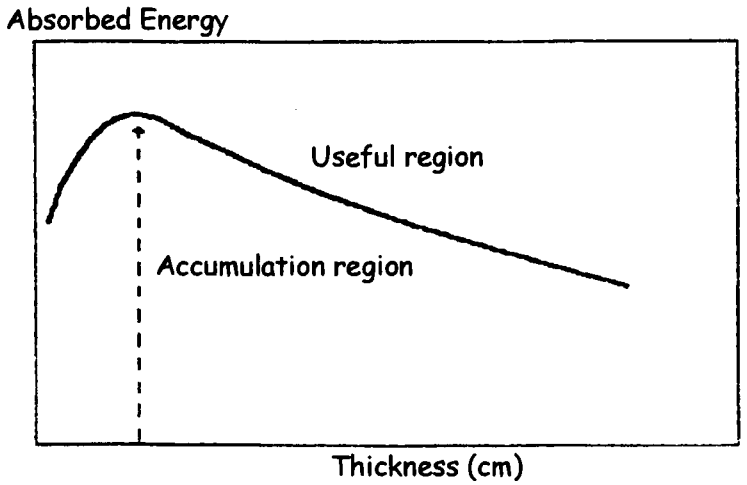

Figure 8: Absorbed dose dependence on sample depth [1].

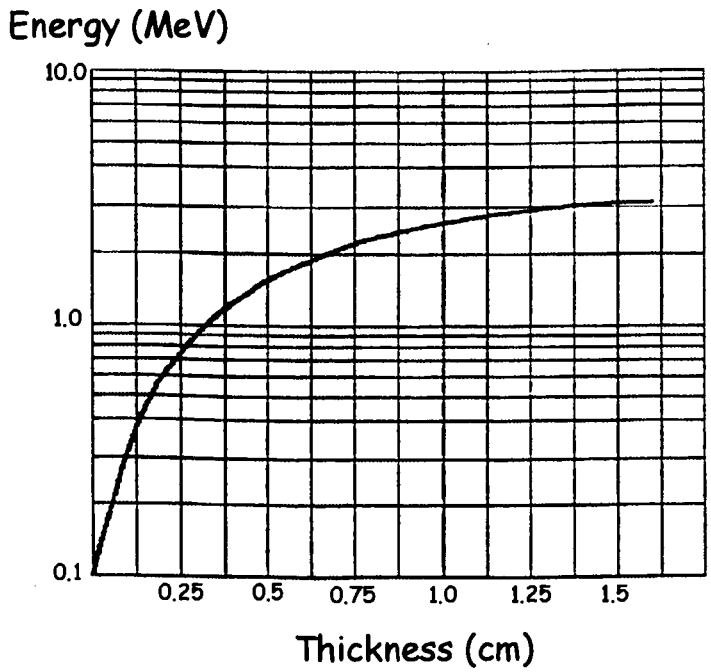

Figure 9: Dependence of the water electronic equilibrium thickness on the photon energy [35]

1.3 Dosimetric methods used for γ radiation

Many physical and chemical parameters undergo variations when they are submitted to irradiation, consequently they can be used to realize a dosimeter, or a system able to measure the absorbed dose.

At Calliope radioisotope source three kinds of dosimeters are used: *Fricke* solution, *Red Perspex* and *alanine* dosimeters. Among them, the solid state dosimeter methods (*Red Perspex* and *alanine*) are *relative* measurement methods, periodically calibrated with an absolute dosimeter method, which is represented by Fricke dosimeter.

1.3.1 Fricke dosimeter

In the chemical dosimeter method, absorbed dose is evaluated by measuring the chemical change induced by irradiation in a solution; next, the measured value will be converted in the dose absorbed by other materials.

One of the most famous and used chemical dosimeters is the Fricke method, whose functioning is based on the radiation induced oxidation of ferrous ions to ferric ($Fe^{2+} => Fe^{3+}$) in conditions of low pH value and in presence of oxygen.

The Fricke dosimeter is an absolute method because it allows to deduce the absorbed dose directly by measuring its optical density variation during an irradiation process. That dosimeter is characterised by a linear behaviour in the range 20-200 Gy and it is used as primary reference method to calibrate secondary dosimeters (Perspex, alanine..) for radiation fields of γ, X and accelerated electrons. Its response is independent on the absorbed dose in the range 0.1-16 MeV and no effect was observed on the measurement precision in the dose rate range 0.2 Gy/s-10^7 Gy/s. During the irradiation procedure, temperature variation between 1 and 60 °C scarcely influences the dosimeter response and the corrections can be neglected.

The dose interval measurable with Fricke dosimeter is between 20 and 400 Gy: in fact, the oxidation induced by a dose lower than 20 Gy is not sufficiently high to be accurately measured. The highest limit is due to oxygen consumption during the chemical reaction and it can be increased up to 10^5 Gy, modifying the Fricke dosimeter with addition of H_2SO_4: in such way

ferrous ions undergo oxidation without oxygen consumption. Fricke dosimeter is composed of a water solution of $FeSO_4$ {o $Fe(NH_4)(SO_4)_2$} 10^{-3} M, H_2SO_4 0.4 M e NaCl 10^{-3} M [36].
The main reactions happening in the dosimeter during the irradiation are the following:

$$Fe^{2+} + OH^{\bullet} \rightarrow Fe^{3+} + OH^{-} \tag{7}$$

$$H^{\bullet} + O_2 \rightarrow HO_2^{\bullet} \tag{8}$$

$$Fe^{2+} + HO_2^{\bullet} \rightarrow Fe^{3+} + HO_2^{-} \tag{9}$$

$$HO_2^{-} + H^{+} \rightarrow H_2O_2 \tag{10}$$

$$Fe^{2+} + H_2O_2 \rightarrow Fe^{3+} + HO^{-} + OH^{\bullet} \tag{11}$$

Every hydrogen atom causes the formation of an hydroperoxide ($HO_2^{\bullet}$), which in turn oxides three ferrous ions according to reactions (9), (10) and (11). Moreover, every hydroxyl radical oxides a Fe^{2+}ion and every hydroperoxide molecole oxides two Fe^{2+}ion. The radiolitic yield (moli/J) can be expressed with the following expression:

$$G\left(Fe^{3+}\right) = 2G_{H_2O_2} + 3G_H + G_{OH} \tag{12}$$

Using a ^{60}Co source, $G(Fe^{3+})$ is equal to 1.61 μmoli/J.
The quantitative analysis of the Fe^{3+} concentration induced by ionising radiation in Fricke dosimeter is performed by measuring the solution absorbance at 304 nm. In particular, for a Fricke dosimeter composed of an oxygenated solution of $Fe(NH_4)(SO_4)_2$ 10^{-3} M, NaCl 10^{-3}M and H_2SO_4 0.8 N, the relation between absorbed dose (Gy) and absorbance measurement is the following:

$$D_{Gray} = \frac{\Delta(OD)}{\varepsilon * G\left(Fe^{3+}\right) * \rho * l} \tag{13}$$

where:
- $\Delta(OD)$ è the optical density variation of solution due to irradiation;
- ε is the molar extinction coefficient of ferrous ions at 304 nm ($E(Fe^{3+} @ 25°C) = 220 \pm 2 m^2 M^{-1}$ a 304 nm) [37];
- $G(Fe^{3+})$ is the number of ferric ions produced per unit of absorbed energy (expressed in 100 eV unit) calculated in $(1.61 \pm 0.02)10^{-6}$ $M \cdot J^{-1}$ for ^{60}Co radiation;
- ρ is the density of the irradiated solution 1024 $Kg \cdot m^{-3}$;
- l is the optical path, equal to 0.01 m.

The role of the NaCl in the Fricke dosimeter is to reduce negative effects of possible organic impurities on the system answer, as it is described in the reference standard [36].
From a solution of H_2SO_4 0.8 N and an absorption cell of 1 cm, equation (13) becomes:

$$D_{Gray} = k * \Delta(OD) = (276 \pm 6) * \Delta(OD) \tag{14}$$

where:

$$\Delta(OD) = (A_l - A_0) - (A_c - A_0) \quad (15)$$

In (15) A_l is the absorbance of irradiated dosimeter, A_c is the control absorbance of dosimeter before irradiation and A_0 is the intrinsic absorbance of the container. Equation (14) turned out to be in perfect agreement with the result of dosimeter calibration performed at the *"Istituto Nazionale di Metrologia delle radiazioni ionizzanti"* (ENEA-Casaccia).

1.3.2 Red Perspex Dosimeter

Solid state dosimeters, such as photographic films, solid scintillators and opportunely doped plastic materials are diffusively used since many years. Their functioning is based on the variation of their coloration due to treatment with different particles (γ-rays, electrons...). Plastic dosimeters offer several advantages which allow a large use of them: reduced dimensions, tissue-equivalent properties, answer independent on dose rate and great reproducibility.

Red 4034 Perspex dosimeters[2] used at Calliope irradiation source are a particular variety of polimethylmetacrilate (PMMA) whose applicability range lies between 5-40 kGy [38]. Perspex dosimeter is a *relative* method, consequently it needs a calibration with an absolute dosimeter method, which in our case is the Fricke dosimeter.

The experimental procedure followed to construct the Red Perspex calibration curve consists of two phases:

1) in the first step, a Fricke dosimeter placed inside a sample compartment is positioned in a fixed and reproducible position in the irradiation cell and the dose rate is measured in that position;
2) in the second step, two groups of Red 4034 Perspex dosimeters undergo irradiation at the doses of 5, 10, 20, 30, 43 and 50 kGy in the same operative conditions used for Fricke dosimeter method.

Irradiation induces a dosimeter absorbance variation at the wavelength of 640 nm. Hence, to construct the calibration curve *Perspex-Fricke* it is necessary to study for each irradiation step the dependence of the absorbed dose on the specific absorbance of each irradiated dosimeter. Next, assuming the specific absorbance (A) as independent variable, the dose (D) as dependent variable and fitting the curve reported in Figure 10 with a polynomial function, the dose dependence on the measured specific absorbance will be the following:

$$y = -0.18 + 96.4 \cdot x - 116 \cdot x^2 + 877 \cdot x^3 + 1082 \cdot x^4 \quad (16)$$

[2] *Red Perspex* dosimeters used at Calliope plant are produced at the *Irradiation and Dosimetry Service, Chemistry Division, Building 10.30,* Aere Harwell, Didcot (Oxfordshire) and they below Batch AJ set.

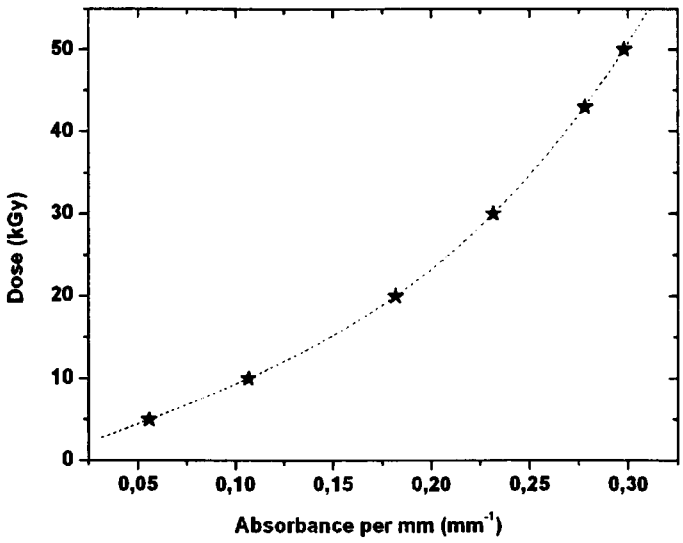

Figure 10 : Experimental data fit with a polynomial curve

1.3.3 Alanine dosimetric method

The alanine dosimeter method is considered one of the most powerful dosimeter techniques and it is based on the detection of stable free radicals induced by ionising radiation in the α-alanine amino-acid, by the Electron Spin Resonance (ESR) [39].

In fact, the irradiation of alanine amino-acid (CH_3-$CHNH_2$-COOH) induces the formation of CH_3-$\dot{C}$H-COOH free radical stable at room temperature. In Figure 11 we reported the ESR spectrum of that radical: as it can be seen, five characteristic peaks are evident due to the interaction between external magnetic field and the odd electron of the molecule.

Figure 11: ESR spectrum of the irradiated α-alanine [39].

The area of the absorption curve is proportional to the number of radiation induced radicals; hence, considering that spectrometer provides the absorption curve derivative of the measured sample, the absorption curve should be integrated two times in order to obtain a size proportional to the number of radiation induced radicals. It can be demonstrated that absorbed energy is proportional to the resonance peak amplitude of the recorded curve, consequently it will be able to extrapolate the energy absorbed by a dosimeter simply by measuring the resonance peak amplitude.

Alanine dosimeter method offers several advantages, such as stability, high dynamic dose range (1 Gy- 500 kGy) no dependence on dose rate and on environment effects as light, humidity and temperature. Moreover, powder alanine can be compressed in little pastilles which can be irradiated with the material under study.

At Calliope plant, alanine dosimeter is calibrated on the absolute Fricke dosimeter. ASTM standards [39] to be followed for the alanine dosimeter calibration on Fricke, establish two different EPR parameter set-ups, in conformity with a dose value lower or higher than 500 Gy (Tables II e III). For that reason, at Calliope plant two alanine calibration curves are used with respect to Fricke: one for low doses (< 500 Gy) and the other for high doses (> 500 Gy).
Dosimeters used for low dose calibration are described in Table IV, while the ones adopted for the high dose calibration are described in Table V.

Table II: ASTM Instrument parameters for low doses (<500 Gy) [39]

Power (mW)	7.92
Sweep width(G):	200
Modulation (G):	10.1
Sweep time (s):	21.0
Filter T.C. (ms):	328
Receiver Gain (dB):	5
Receiver Offset:	0
Receiver Phase:	0
Field Offset (G):	8.93
Sweep numbers:	5
Sample Height [3](mm):	15

1.3.3 a - Alanine dosimeter calibration for low doses

To construct the calibration curve for alanine dosimeter at doses lower than 500 Gy, Fricke dosimeter is located in a dosimeter cell in a position fixed and reproducible to measure the absorbed dose in that position. Once dose rate has been evaluated, alanine dosimeter is irradiated at the doses of 3, 10, 20, 46, 54, 80, 117 and 389 Gy in the same operative conditions. Next, the alanine EPR signal is measured with a spectrometer (Bruker EMS104) and it is normalised to the mass. The alanine dosimeters used for low doses (<500 Gy) were produced in Germany, by Dr A.Wieser (MESSTECHNIK, Altomünsterstr. 71, D-80997 München). The dose dependence (D) on the resonance peak to peak amplitude normalised to the mass (hp-p/m) represents the calibration curve, whose interpolation furnishes the dose dependence on the EPR signal (Figure 12):

$$D(Gy) = -3.7 + 111 * \frac{h_{p-p}}{m} \tag{17}$$

Table III: ASTM Instrument parameters for high doses (>500 Gy) [39]

Power (mW)	3.97
Sweep width(G):	200
Modulation (G):	1.01
Sweep time (s):	10.5
Filter T.C. (ms):	81.9
Receiver Gain (dB):	5
Receiver Offset:	0
Receiver Phase:	0
Field Offset (G):	8.93
Sweep numbers:	2
Sample Height:	18

[3] It indicates the sample position within the cavity, equal to $20 - \frac{h}{2}$, where h is the sample height.

Table IV: Composition of dosimeters for low doses

Dosimeter:	AWM230
Materials:	85% wt L-α-alanine 15% wt paraffin wax
Shape:	cylindrical, 4.8 mm diameter and 10 mm length.
Mass:	230 1% (mg)
Density:	1.27 g/cm^3
Dynamic dose range:	1 Gy – 500 kGy
Detection threshold:	0.1 Gy

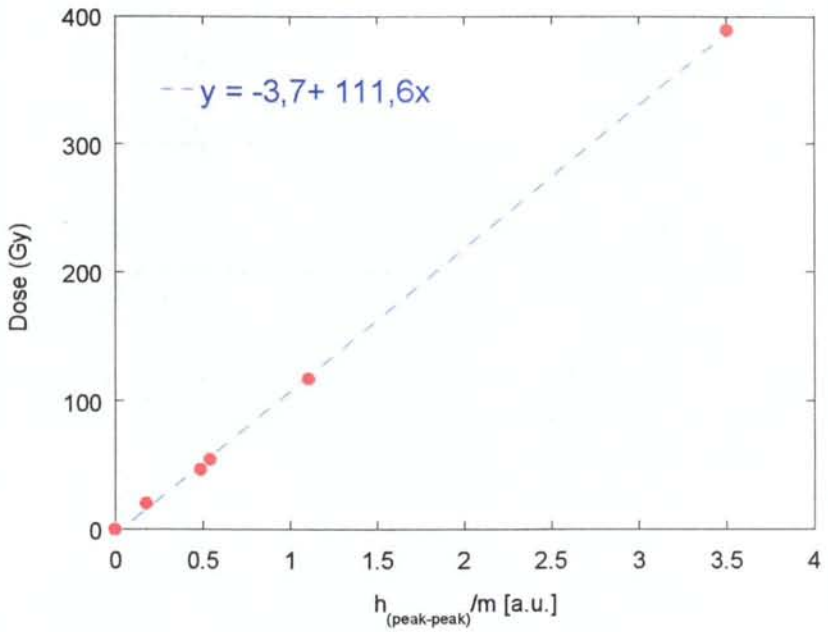

Figure 12: Alanine dosimeter calibration for low doses (< 500 Gy)

1.3.3 b - Alanine dosimeter calibration for high doses

To construct the calibration curve for high doses, *Gold* Bruker dosimeters were used, whose dynamic dose range varies between 500 Gy to 50 kGy and whose properties are reported in Table V. In that case, the irradiation doses are equal to 0.4, 0.8, 1.5, 6 and 23 kGy.

Table V: Composition of dosimeters for high doses

Dosimeter:	Bruker, *Gold* (1% error mass)
Shape:	cylindrical, 4.8 mm diameter and 5 mm height
Mass:	88±1% (mg)
Dynamic dose interval:	500 Gy – 50 kGy

Also for high doses, the dependence of the dose on the EPR signal intensity normalised to the mass is linear and it can be interpolated with the following curve (Figure 13):

$$D(Gy) = -0.31 + 1.99 * \frac{h_{p-p}}{m} \tag{18}$$

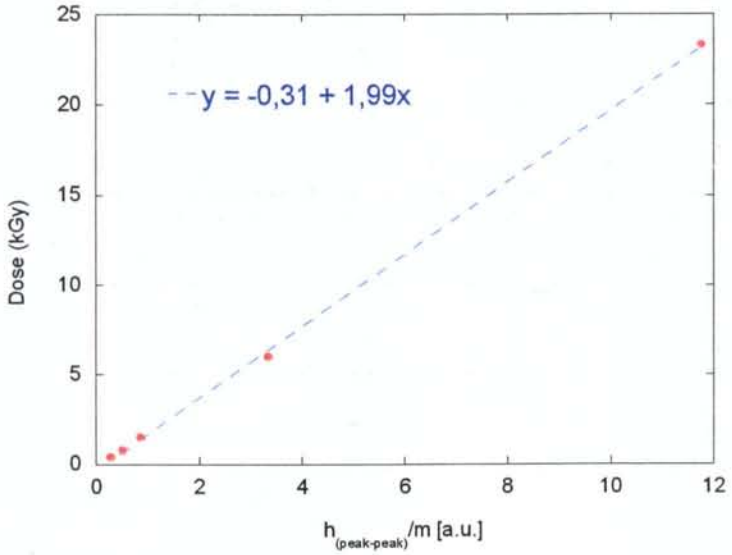

Figure 13: Alanine dosimeter calibration for high doses (>500 Gy)

1.4 Interaction of X-rays and γ radiation with matter

The physical processes involved in the energy transfer mechanism from γ radiation to matter depend on the energy (hν) of the impinging photons and on the material. In the energy range between 0.01 MeV and 100 MeV the dominant processes are:

1. Photoelectric effect;
2. Compton effect;
3. Pair production.

The relative importance of the three processes is reported in Figure 14 in function of the atomic number Z and the photon energy hν [40]. The curves are referred to regions where none of the adjacent effects is dominant.

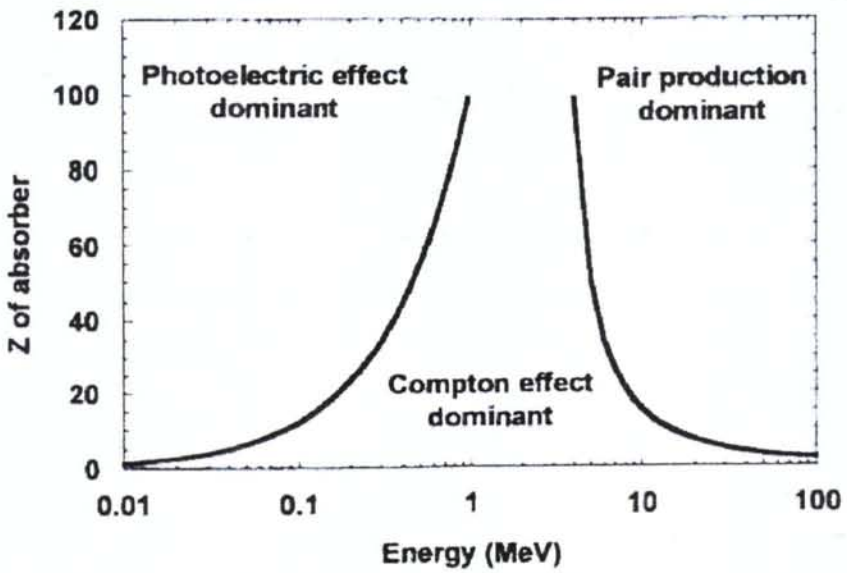

Figure 14: Relative importance of Photoelectric, Compton and Pair production effects [40]

1.4.1 Photoelectric effect

The Photoelectric effect is the emission of an atomic electron after the absorption of an incident quantum hν; the emitted electron is called *"photoelectron"* and it generally belongs to an inner atomic shell. The kinetic energy of the emitted electron (E_{pe}) is given by:

$$E_{pe} = h\nu - E_0 \qquad (19)$$

where hν is the energy of the impinging photon and E_0 is the electron binding energy. The energy E_0 is then converted in characteristic X-rays or Auger electrons, produced when the vacancy created by the emitted electron is filled. X-rays are dominant in high Z elements while Auger electrons are characteristic of light elements: X-rays are generally reabsorbed in a second photoelectric process and the total photon energy is absorbed in the detector. The Photoelectric effect is as much probable as the electron is bonded to the atom. In fact, this process is most probable for electrons belonging to the K shell, which represent the greatest part of the emitted photoelectrons. Moreover, for every shell, the photoelectric emission is as more probable as the photon energy is near E_0. The cross section of this process is monotonically decreasing with photon energy and it is characterised by typical absorption peaks at the photoelectric energy edge of the different shells (M, K, L). The Moseley law defines the energy edge value:

$$E = Rhc\frac{\left(Z-\sigma^2\right)}{n^2} \qquad (20)$$

where Rhc=13.6 eV, Z is the atomic number, σ is the screen constant and n the principal quantum number [41]. As far as the photoelectric cross section is concerned, there is no analytic expression valid for every kind of photon energy. Practically, the adopted methods and the approximations depend on the energy region.

1.4.2 Compton effect

In the Compton effect, a photon with energy around 1 MeV interacts with an atomic electron. The result is the scattering of the photon along a direction different from the incident one, while the electron is diffused with a certain kinetic energy (Figure 15).

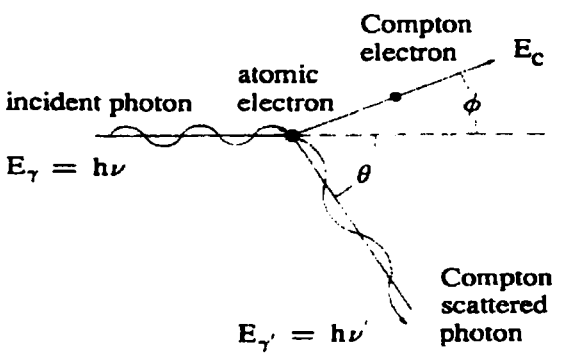

Fig 15: Compton effect

Applying the energy and momentum conservation laws, it is possible to derive that the photon energy after the collision ($E_{\gamma'}=h\nu'$) is related to its initial energy ($E_\gamma=h\nu$) and to the diffusion angle (θ) through this relation:

$$E_{\gamma'} = \frac{E_\gamma}{1+\alpha\left(1-\cos\theta\right)} \qquad (21)$$

where $\alpha = \frac{h\nu}{mc^2} = \frac{E_\gamma}{0.511}$, and E_γ e $E_{\gamma'}$ are expressed in MeV.

The kinetic energy of the Compton electron is given by:

$$E_c = E_\gamma - E_{\gamma'} = \frac{\alpha(1-\cos\theta)}{1+\alpha(1-\cos\theta)} E_\gamma \qquad (22)$$

From the aforementioned relations, it follows that the energy spectrum of the Compton electron ranges from 0 (corresponding to θ=0°) to a maximum value (corresponding to θ=180°) expressed by this relation:

$$E_{c(\max)} = \frac{E_\gamma}{1+\frac{0.511}{2E_\gamma}} MeV \qquad (23)$$

The Compton effect is dominant at energies between 0.8 MeV and 4 MeV [42].

1.4.3 Pair production

In the Pair production process, a photon is completely absorbed and its energy is converted in a couple electron-positron. Due to energy and momentum conservation laws, the process is possible only in the atomic or electronic Coulomb field. The pair production process is an edge-mechanism and it may happen in the atomic nucleus only if $h\nu >> 2m_0c^2$ (1.02 MeV), where m_0 is the rest mass of the electron and c is the light velocity [40, 42]. The quantity of energy transformed in kinetic energy of the couple electron-positron is:

$$E_{e^+} - E_{e^-} = h\nu - 2mc^2 \qquad (24)$$

Between the two particles, the positron tends to acquire more energy than the electron because of the Coulombic repulsion of the nucleus. Then, it annihilates with an atomic electron with the consequent emission of two 0.511 MeV photons. The Pair production process may also happen in the Coulombic field of the atomic electron. That process is greatly less probable than the one taking place in the nucleus field and it is characterised by edge energy of 4 m_0c^2. The cross-section related to this process is given by:

$$\tau = 4Z^2\alpha r_e^2 f(E,Z) \qquad (25)$$

where f(E,Z) is a slowly varying function depending on the screen level offered by electrons, α is the hyperfine constant and r_e is the classical electron radius [43]. The photon mean free path before its conversion to the couple (e^+-e^-) is given by:

$$\lambda_{pair} = \frac{1}{N\tau} \qquad (26)$$

where N in the number of atoms in the unitary volume and τ is the cross section related to the pair production; it is related to the radiation length through this expression:

$$\lambda_{pair} = \frac{9}{7} L_{rad} \qquad (27)$$

where the radiation length indicates the mean free path after which an electron reduces its initial energy of a factor *e*, through the *Bremsstrahlung* radiation.

1.5 Absorbed dose calculation

To calculate the energy deposition and the penetration of photons (x-ray, γ-ray, *bremsstrahlung*) in biological, shielding and other materials, it is necessary to introduce the basic quantities mass attenuation coefficient $\left(\frac{\mu}{\rho}\right)$ and mass energy-absorption coefficient $\left(\frac{\mu_{en}}{\rho}\right)$.

The mass attenuation coefficient is defined as:

$$\frac{\mu}{\rho} = \frac{1}{x} \cdot \ln\left(\frac{I_0}{I}\right) \qquad (28)$$

where I_0 is the incident intensity of a monoenergetic photon flux, penetrating a layer of material with mass thickness x and density ρ and emerging with intensity I.
The mass energy-absorption coefficient involves the further emission of radiation produced by charged particles when they travel through the medium, and it is defined as:

$$\frac{\mu_{en}}{\rho} = (1-g) \cdot \frac{\mu_{tr}}{\rho} \qquad (29)$$

where g factor represents the average fraction of the kinetic energy of secondary charged particles (produced in all the types of interactions) that is subsequently lost in radiative energy-loss processes as the particles slow to rest in the medium and $\frac{\mu_{tr}}{\rho}$ is the mass energy-transfer coefficient.
Knowing the mass energy absorption coefficient it is possible to convert the absorbed doses in the Fricke dosimeter (water) to doses absorbed in other materials through the following relationship:

$$D_m = \frac{\left(\frac{\mu_{en}}{\rho}\right)_m}{\left(\frac{\mu_{en}}{\rho}\right)_{H_2O}} \cdot D_{H_2O} \qquad (30)$$

where D_{H_2O} is the dose absorbed in water and $\left(\frac{\mu_{en}}{\rho}\right)$ is the mass attenuation coefficient.

As an example, if dose absorbed in air is required, the previous formula (for ^{60}Co field) will become the following:

$$D_{aria} = \frac{\left(\frac{\mu_{en}}{\rho}\right)_{aria}}{\left(\frac{\mu_{en}}{\rho}\right)_{H_2O}} \cdot D_{H_2O} = \frac{2.666 * 10^{-2} (cm^2/g)}{2.965 * 10^{-2} (cm^2/g)} = 0.899 * D_{H_2O} \qquad (31)$$

When silicon based electronic devices are irradiated, it will be useful to know the conversion factor of the dose absorbed in water with respect to dose absorbed in silicon:

$$D_{Si} = \frac{\left(\frac{\mu_{en}}{\rho}\right)_{Si}}{\left(\frac{\mu_{en}}{\rho}\right)_{H_2O}} \cdot D_{H_2O} = \frac{2.652 * 10^{-2} (cm^2/g)}{2.965 * 10^{-2} (cm^2/g)} = 0.894 * D_{H_2O} \qquad (32)$$

The mass attenuation coefficients used in (31) and in (32) are reported in [44].
For non homogeneous materials, the mass attenuation coefficient can be evaluated by the following relationship:

$$\left(\frac{\mu_{en}}{\rho}\right)_m = \sum_{i=1}^{N} w_i * \left(\frac{\mu_{en}}{\rho}\right)_i \qquad (33)$$

where $\left(\frac{\mu_{en}}{\rho}\right)_i$ and w_i are the mass attenuation coefficient and the atomic weight fraction of each i-atomic specie inside the sample.

In the case of high dimension objects, it could be useful to know the dose distribution inside the thickness. In conditions of charge particle equilibrium conditions and under the hypothesis that secondary charged particles loose energy only through collision processes (as at ^{60}Co energies), the dose absorbed in a material coincides with *kerma*, K, which represents the sum of the initial kinetic energies of all the charged particles liberated by uncharged ionizing radiation (neutrons and photons) in a sample of matter, divided by the mass of the sample.
Consequently, knowing the *kerma* behaviour throughout a certain material thickness:

$$K = K_0 * B * e^{-\mu x} \tag{34}$$

it is possible to know also the absorbed dose behaviour inside the material:

$$D = D_0 * B * e^{-\mu x} \tag{35}$$

where D_0 is the dose on the material surface, B is the *build-up* factor and μ is the linear attenuation coefficient at a certain energy.
As an example, Figure 16 reports the mass attenuation coefficient and the mass energy absorption for silicon:

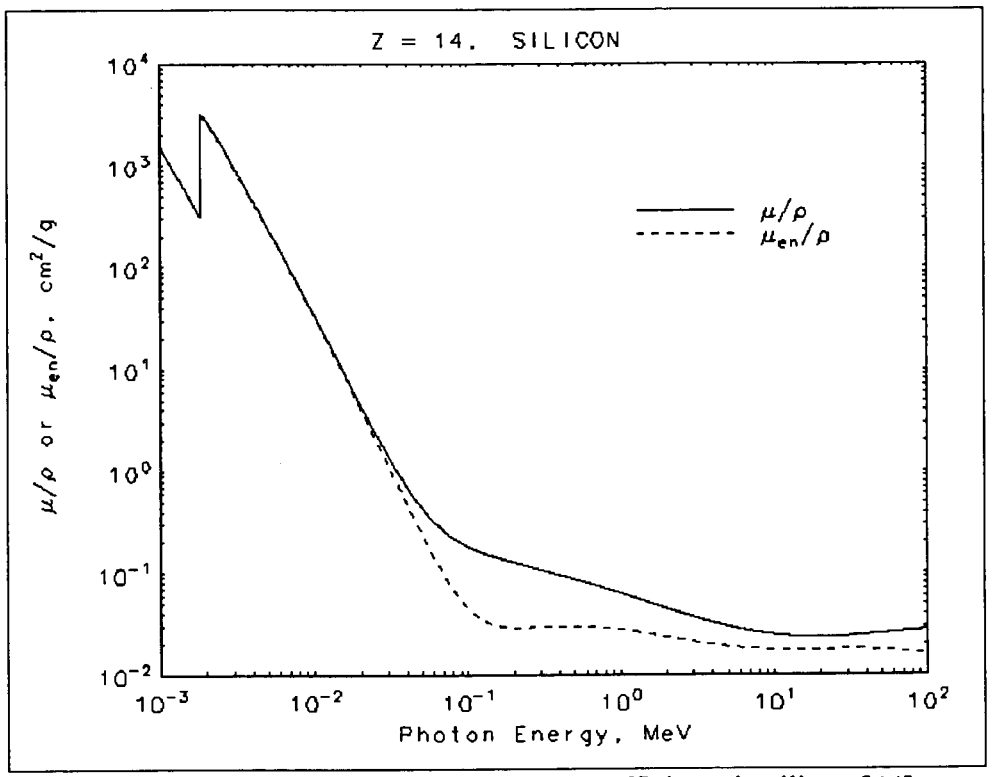

Figure 16: Attenuation and absorption coefficients in silicon [44]

Chapter 2: Ionising radiation damage test on electronic devices at Calliope plant

2.1 Radiation induced damage on electronic devices

With the advent of new High Energy Physics and Astrophysics experiments where electronic systems are exposed to high fluxes of energetic particles [45]-[52], the interest on electronic device radiation damage has increased more and more.

The physical processes involved in the radiation damage of electronic devices are particularly complex and they depend on several parameters, such as the kind of radiation, energy and fluence. In general they can be grouped in two classes: 1) ionization damage; 2) bulk damage.

The ionization damage, also called surface damage, is caused by electron-hole pairs generated in silicon dioxide (SiO_2) and other insulators by ionizing radiation. In SiO_2, electrons are much more mobile than holes and they are quickly collected at the positive electrode, even if some fraction of them recombine with holes. The charge yield, i.e. the fraction of the electron-hole pairs surviving the initial recombination, depends on the type and energy of the impinging particles. The holes, escaping the initial recombination, are relatively immobile and they slowly undergo a hopping transport between localized sites in the oxide in presence of an electric field. Some of them can be trapped giving rise to accumulation of positive charge in the oxide or can generate interface states at the SiO_2/Si interface, so affecting the device operation.

The bulk damage or displacement damage is caused by collisions of energetic protons, neutrons, ions and electrons, which transfer sufficient energy to knock out a Si atom from its lattice position. A vacancy-interstitial pair called Frenkel defect is so generated, which migrates until a stable defect is formed by association with other defects, impurities or dopants.

2.2 MIL-STD-883 and ESA/SCC BASIC Specifications

At Calliope plant it is possible to perform ionizing damage test on electronic components according to procedures defined in MIL-STD-883 and in ESA/SCC BASIC Specifications No.22900. The difference between the two protocols is that MIL-STD-883 defines the procedures to test electronic devices to be used in Military and Aerospace electronic systems, while ESA/SCC BASIC Specifications No.22900 are strictly devoted to the qualification of integrated circuits and discrete semiconductors suitable for Space applications.

As far as the adopted dose rate concerned, according to MIL specifications (standard conditions) the dose rate has to lie between 50 rads(Si)/s and 300 rads(Si)/s (i.e., between 0.5 Gy(Si)/s and 3 Gy(Si)/s) and it has not to vary more than ±10% during each irradiation.

In ESA specifications, two dose rate windows can be adopted:

1) the standard dose rate between 3.6 krad(Si) and 36 krad(Si)/h (i.e., between 36 Gy(Si)/h to 360 Gy(Si)/h);

2) the low dose rate between 36 rad(Si)/h and 360 rad(Si)/h (i.e., between 0.36 Gy(Si)/h and 3.6 Gy(Si)/h).

Depending on the expected maximum dose rate, the total irradiation time must be less than 96 hours. The time interval between the end of the irradiation and the beginning of the device electrical characterization has to be less than 1 hour. Moreover, the time interval between one irradiation step and the beginning of the next exposure must be at most 2 hours. After irradiation, the eventual accelerated aging have to be performed keeping the component under bias and at 100 °C for 1 week [53]-[55].

During the irradiation procedure test specimens have to be surrounded by equilibrium material, which will minimize dose enhancement from low energy scattered radiation by producing charge particle equilibrium. To this purpose, both MIL and ESA specifications recommend the use of a container of at least 1.5 mm Pb with an inner lining of at least 0.7 mm Al. In fact, considering the fraction of attenuated photons as a function of energy and thickness for Pb (Figure 17) and Al (Figure 18), we can easily evict that the 1.5 mm Pb (0.7 mm Al) layer absorbs 95% (99%) of the

photons having energy lower than 150 keV (15 keV). The Pb/Al container also produces approximate charged particle equilibrium for silicon devices.

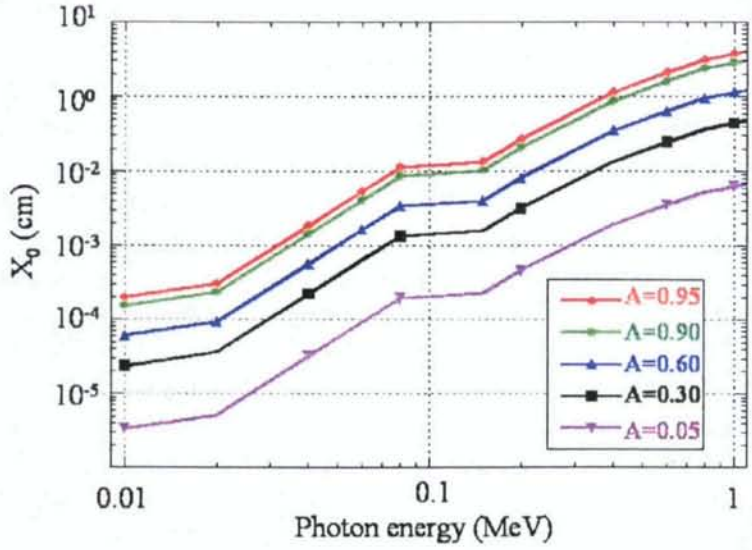

Figure 17. Pb thickness as a function of the photon energy to attenuate the photons at the percentage value reported in the inset.

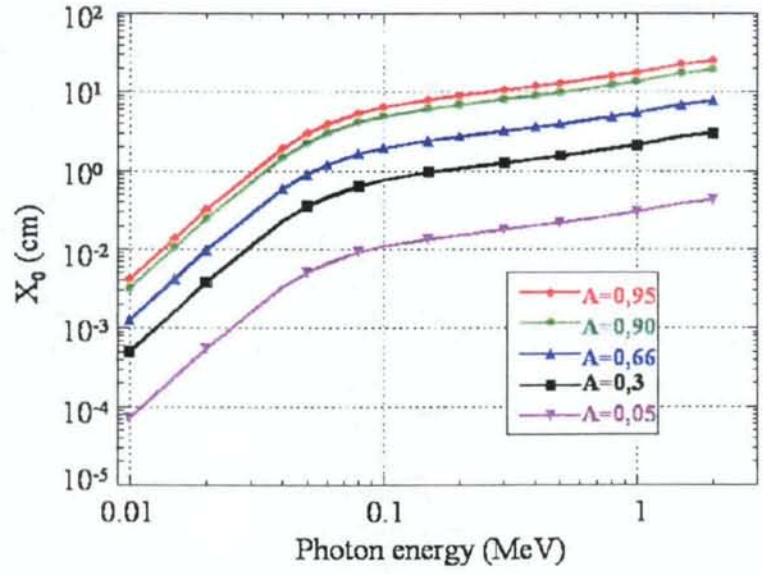

Figure 18. Al thickness as a function of the photon energy to attenuate the photons at the percentage value reported in the inset.

Chapter 3: Simulation of Calliope radiation field with FLUKA code

3.1 Dose rate theoretical estimation and comparison with experimental results

To map the γ radiation field inside the irradiation cell, we have performed a simulation of Calliope dose rate profile by using FLUKA code in collaboration with Dr Mika Huhtinen (CERN, Switzerland) [56]. Such code includes a good description of the electromagnetic physics down to about 1\,keV and its models are adapted and extended versions of the EGS4 shower code.
Knowing accurately the properties of ^{60}Co decay and the material distribution in the source and its surroundings an accuracy of better than 10 percent can be expected from such a simulation. By far the dominant uncertainties come from the amount of material in the source rods themselves and the support rack. In fact, whereas the activities are exactly known there is some uncertainty about the exact size and density of the rods. Another source of uncertainty is the double encapsulation described in the simulation which might not be exactly conform to reality.
As reported in the rack supporting the rods was described as an assembly of 2 mm thick steel rings joined by vertical steel bars and the room was assumed to be empty of any other material, except for the pool and the footbridge. ^{60}Co decays were simulated such that each decay emitted one photon of 1173.237 keV and another of 1332.5 keV independently in a random direction. The probability for emission within a given source rod was determined according to the activity of the rod and the position of decay within the rod was sampled randomly within the active area.
At the ^{60}Co energies, the dose is the amount of ionising energy deposited in matter by electrons produced by γ photons via photo-electric effect, Compton scattering of pair production, where all these reactions depend on the characteristics of the medium. Thus, as soon as any material is introduced into the empty room, the dose will locally change.
With the available CPU power it was not possible to calculate the dose in air directly from the ionisation of the electrons. The energy-dependent mass-energy absorption coefficient can be used in the simulation to calculate the dose directly from the photon flux. In our simulations we adopted the coefficients for water, consequently the results should give the best approximation for the dose measured by a 'water-equivalent' detector positioned in the room.
In Figure 19 we reported the detail of the simulated radiation field inside the ^{60}Co pencil rack and in the region closest to the source. On the contrary, Figure 20 and Figure 21 represent the dose rate distribution in the overall irradiation cell: the first image reports the top view x-y of the dose rate profile and the second one shows the lateral y-z dose rate profile inside the radiation cell.
To validate the Calliope γ radiation field simulation, in our laboratories we have performed experimental dosimetric measurements in two dosimetric positions (72 cm and 320 cm) where the expected theoretical dose rates were equal to 350 and 17 Gy/h, respectively. Table VI shows the comparison between the theoretical and experimental results, which turned out to be in good agreement.

Table VI: Theoretical and Experimental dose rate

Distance from centre of the source (cm)	Theoretical dose rate in water (Gy/h)	Experimental dose rate in water (Gy/h)
75	350	378
350	17	19.9

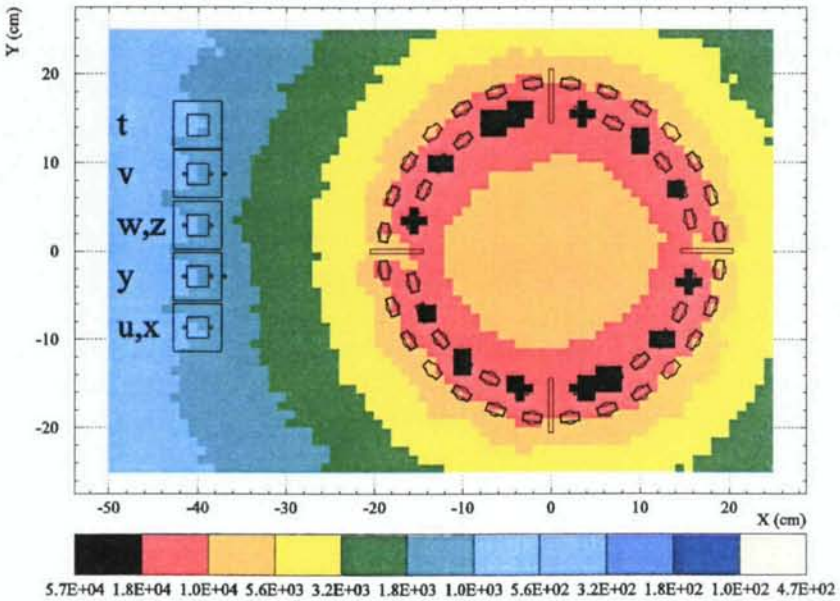

Figure 19: Top view x-y of the dose rate profile represented by colour code (Gy/h) in region near the source

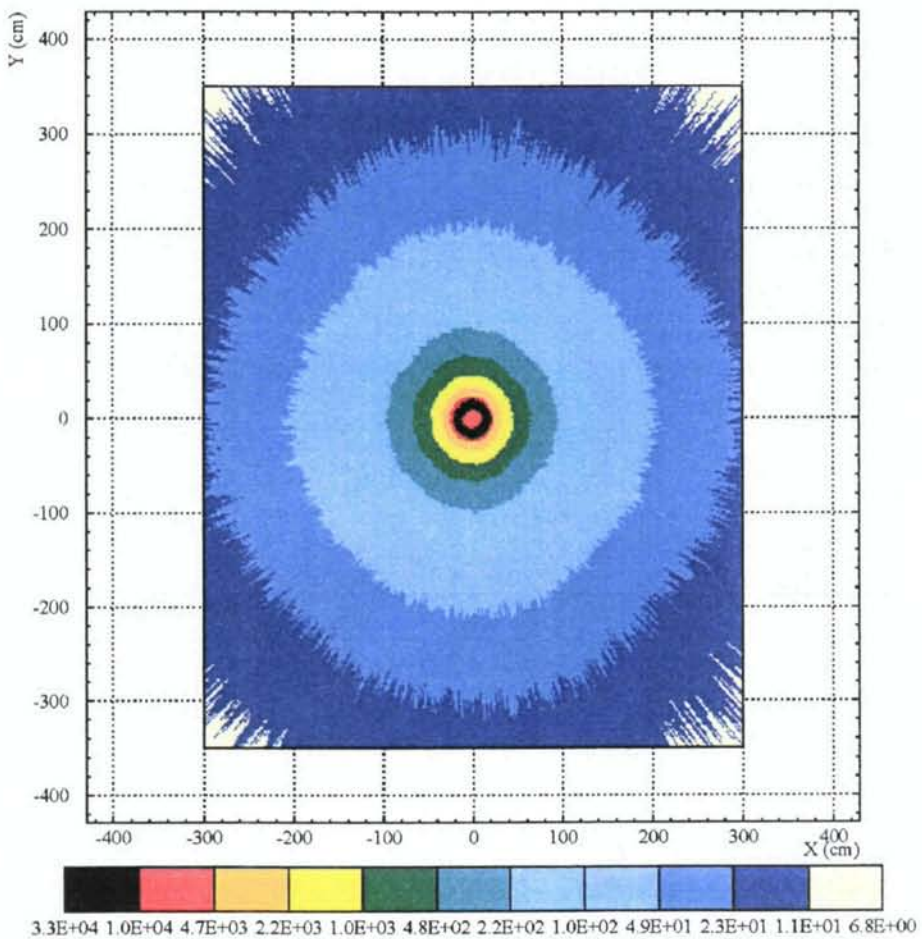

Figure 20: Top view x-y of the dose rate profile represented by colour code (Gy/h) inside the irradiation cell.

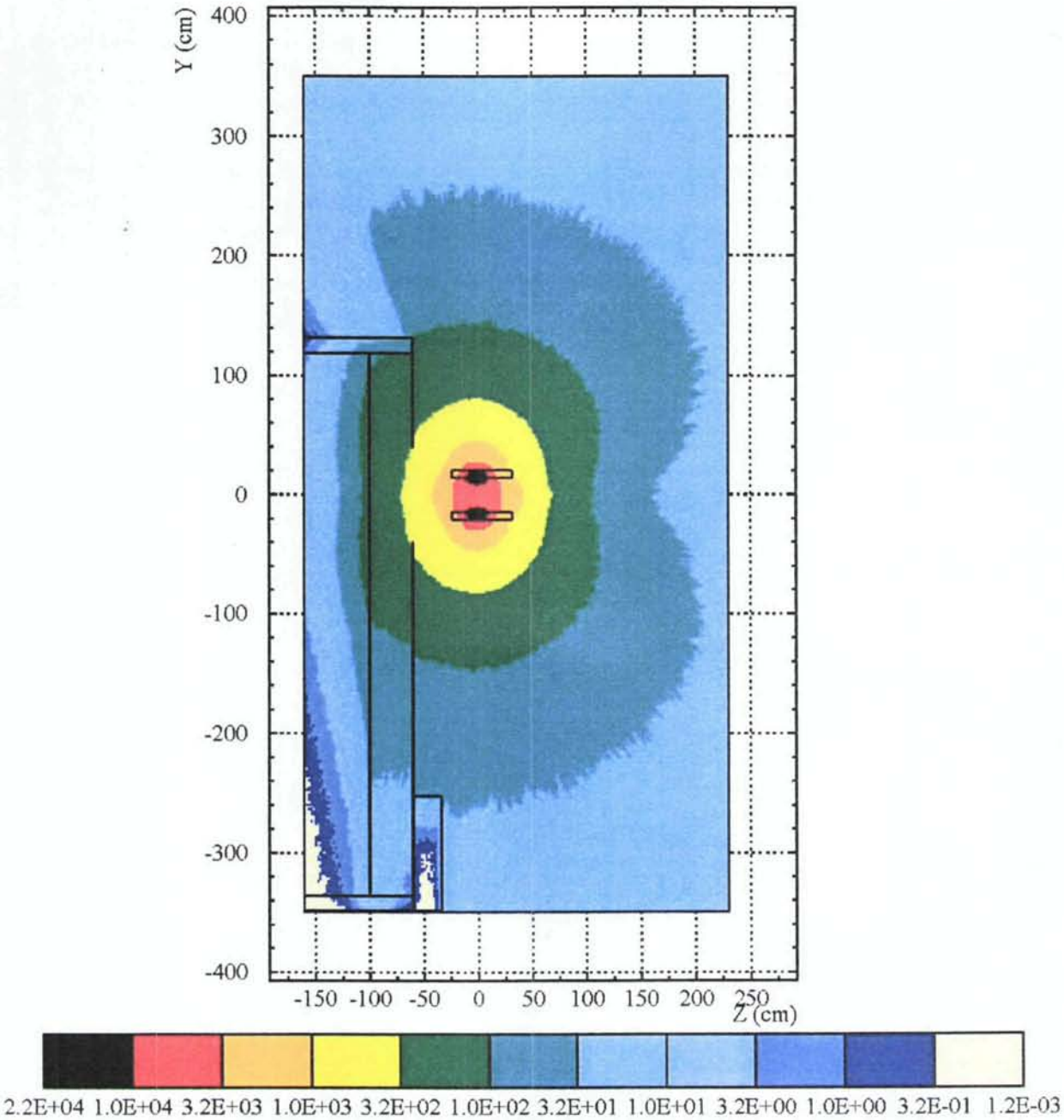

Figure 21: Lateral y-z dose rate profile represented by colour code (Gy/h) inside the radiation cell.

Acknowledgements

Authors are grateful to Dr Mika Huhtinen (CERN, Switzerland) for having provided the simulation of the Calliope γ radiation field and to the Director of Calliope plant (Dr Armando Festinesi, FIS-ION, ENEA-Casaccia Research Centre) for the continuous support and encouragement during the realisation of this work.

Moreover, they thank Mr Antonio Lucchi (FIS-ION, ENEA-Casaccia Research Centre) for the mechanical support in the realisation of the steel platform, movable arc measurers and movable mountings, thanks to which the potentialities of the plant were strongly improved.

REFERENCES

[1] Roesch W., Attix F.H., "Basic concepts of dosimetry", in *Radiation dosimetry*, New York, Roesch W., Attix F.H. (eds), Academic Press, 1968.

[2] Pelliccioni M., "Elementi di dosimetria delle radiazioni", ENEA, 1983.

[3] ASTM E 170-76, "Standard Definitions of Terms relating to Dosimetry", 1976.

[4] Baccaro S., Borgia B., Festinesi A., "Gamma and neutron irradiation facilities at Enea Casaccia Centre (Rome)", Report Cern-CMS/TN, 95-192 (RADH), 1995.

[5] S. Baccaro, *"Radiation damage session"* Convenor's report, in Proceedings of the 8th International Conference on "Astroparticle, Particle and Space Physics, Detectors and Medical Physics Applications", Villa Olmo, Como, Italy, 6-10 October 2003, edited by M. Barone, E. Borchi, J. Huston, C. Leroy, P. G. Rancoita, P. Riboni & R. Ruchti, World Scientific Edition, 2004.

[6] S. Baccaro, U. Buontempo and P. D'Atanasio, "Radiation induced degradation of EPR by IR oxidation profiling" Rad. Phys. Chem., Vol.42, pp.211-214, 1993.

[7] S. Baccaro, B. Caccia, S. Onori, M. Pantaloni, "The influence of dose rate and oxygen on the irradiation induced degradation in ethylene-propylene rubber" NIMB, 105, pp. 97-99 (1995).

[8] S. Baccaro, L.A. Pajewski, G. Scoccia, R. Volpe, J.M. Rosiak, "Mechanical properties of polyvinylpyrrolidone (PVP) hydrogels undergoing radiation" NIMB 105, pp. 100-102, 1995.

[9] P. Anelli, S. Baccaro, M. Carenza, G. Palma, "Radiation Grafting on hydrophilic monomers onto ethylene-propylene rubber", Rad. Phys. Chem. Vol. 46, No 4-6, pp. 1031-1035, 1995.

[10] S. Baccaro, K. Blazek, F. de Notaristefani, P. Maly, J.A. Mares, R. Pani, R. Pellegrini, A. Soluri, "Scintillation properties of YAP:Ce" NIMA 361, pp. 209-215, 1995.

[11] S. Baccaro, "Radiation induced effects in ethylene-propylene copolymer with antioxidant" in "Irradiation of Polymers" Eds by R.L. Clough and S.W. Shalaby, American Chemical Society Series 620, pp. 323, 1996.

[12] S. Baccaro, G. De Cesare, A. Ferrari, G. Maiello, M. Montecchi, M. Petti, "Conductivity effects in amorphous hydrogenated silicon film induced by gamma-ray irradiation", Sensors and Actuators B, 31, pp. 107, 1996.

[13] S. Baccaro, B. Bianchilli, C. Casadio, G. Rinaldi, "Radiation induced effects on Particulate Composites from Epoxy Resin and Fly-Ash" Rad. Phys.Chem. Vol.52, No. 1-6, pp. 187-192, 1998.

[14] S. Baccaro, A. Cecilia, M. Montecchi, T. Malatesta, F. De Notaristefani, S. Torrioli, F. Vittori "Refractive index and absorption length of YAP:Ce scintillation crystal and reflectance of the coating using in YAP:Ce^{3+} single-crystal matrix", NIMA 406, pp. 479-485, 1998.

[15] F. Cataldo, Y. Keheyan, S. Baccaro, "The effect of gamma-irradiation on anthracite coal and bitumen" Journal of Radioanalytical and Nuclear Chemistry, Vol. 262, No. 2, pp. 443-450, 2004.

[16] F. Cataldo, Y. Keheyan, S. Baccaro, "Gamma radiolysis of chiral molecules: R(+) limonene, S(-) limonene and R(-)-α-phellandrene" Journal of Radioanalytical and Nuclear Chemistry, Vol. 262, No. 2, pp. 423-428, 2004.

[17] F. Xia, S. Baccaro, D. Zhao, M. Falconieri, G. Chen, "Gamma ray Irradiation Induced Optical Band Gap Variations in Chalcogenide Glasses, accepted by NIMB.

[18] S. Baccaro, A. Cemmi, C. Colombi, M. Fiocca, G. Gambarini, B. Lietti, G. Rosi, "In phantom dose mapping in neutron capture therapy by means of solid state detectors", NIMB 213, pp. 666-669, 2004.

[19] A. Cecilia, S. Baccaro, A. Cemmi, V. Colli, G. Gambarini, G. Rosi, L. Scolari, "Alanine and TLD coupled detectors for fast neutron dose measurements in Neutron Capture Thererapy (NCT)", Radiation Protection Dosimetry Vol. 110, Nos 1-4, pp. 637-640, 2004.

[20] G. Chen, Y. Yang, D. Zhao, F. Xia, "Composition Effects on Optical Properties of Tb^{3+}-doped Heavy Germinate Glasses", J. Am. Ceramic Soc. 88 [2], pp. 293-296, 2005.

[21] A. Cecilia, S. Baccaro, A. Piegari, I. Di Sarcina, "Optical coatings behaviour under γ irradiation for space applications", Proc. SPIE Vol. 5494, pp. 529-535, 2004.

[22] M. Kobayashi, Y. Usuki, M. Ishii, N. Seguttuvan, K. Tanji, M. Chiba, K. Hara, H. Takano, M. Nikl, P. Bohaceck, S. Baccaro, A. Cecilia, M. Diemoz, "Significant improvement of $PbWO_4$ Scintillating Crystals by Doping with Trivalent ions", NIMA 434, pp. 412-423, 1999.

[23] S. Baccaro, P. Bohacek, A. Cecilia, M. Montecchi, E. Mihokova, M. Nikl, "Effect of La doping on Calcium Tungstate ($CaWO_4$) crystals radiation hardness", Phys. Stat. Sol. (a) 178, pp. 799, 2000.

[24] S. Baccaro, A. Cecilia, A. Cemmi, G. Chen, E. Mihokova, M. Nikl, "Optical characterisation under irradiation of Ce^{3+} (Tb^{3+})-doped phosphate scintillating glasses", IEEE Trans. Nucl. Science, Vol. 48, NO3, 2001.

[25] S. Baccaro, A. Cecilia, G. Chen, J. Mares, E. Mihokova, M. Nikl, P. Polato, G. Zanella, R. Zannoni, "Effect of γ irradiation on optical properties of Ce^{3+} doped phosphate and silicate scintillating glasses", Rad. Phys. Chem., Vol. 63/ 3-6, pp. 227-230, March 2002.

[26] S. Baccaro, A. Cecilia, G. Chen, Y. Du, L. Nencini, S. Wang, "Optical transmittance and irradiation resistance of rare-earth (Ce^{3+}, Tb^{3+}, Pr^{3+}) doped heavy germanate glasses", Radiation Effects and Defects in Solids, Vol. 158, pp. 451-456, 2003.

[27] S. Baccaro, V. Brunella, A. Cecilia, L. Costa, "Gamma irradiation of Poly (Vinyl Chloride) for medical applications", NIMB, 208C pp. 195-198, 2003.

[28] S. Baccaro, F. Cataldo, A. Cecilia, A. Cemmi, F. Padella, A. Santini, "Interaction between reinforce carbon black and polymeric matrix for industrial applications", NIMB, 208C, pp. 191-194, 2003.

[29] S. Baccaro, A. Cecilia, A. Venezia, A. Fedorov, M.V. Korzhik, A. Barisevich, V. Domenev, "Radiation damage of $REAlO_3:Ce^{3+}$(RE=Y, Lu) scintillators under γ and neutron irradiation", NIMA 537, pp. 431-434, 2005.

[30] S. Baccaro, A. Cecilia, D. Passaro, "ESR dating of Middle Pleistocene coral", will be presented at LED2005 Conference, which will be held in Cologne 24-29 July 2005.

[31] Y. Tabata, Y. Ito, S. Tagawa, Handobook of Radiation Chemistry, CRC Press, 1991.

[32] A.R. Rutledge, L.V. Smith, J.S. Merrit, NIMA 206, pp. 211, 1983.

[33] ICRU Report 33- Radiation Quantities and Units, 1980.

[34] PELLICCIONI M., "Fondamenti fisici della radioprotezione", Bologna, Pitagora editrice, 1993.

[35] Norma I.E.C. 15B.4.1, 1994.

[36] ASTM E 1026-95, "Standard Practice for Using the Fricke Reference Standard Dosimetry System", 1995.

[37] D. Mosse et al., Phys. Med. Biol. 1982 Vol.27 n° 4, 583-596.

[38] ASTM E 1276-96, "Standard Practice for Use of Polymethylmethacrylate Dosimetry System", 1996.

[39] ASTM E 1607-96, "Standard Practice for Use of the Alanyne-EPR Dosimetry System", 1996.

[40] Price W.J., Rivelazioni delle radiazioni nucleari, Bulzoni Editore, Roma, 1972.

[41] Segre' E., Nuclei e particelle, Zanichelli, Bologna, 1982.

[42] Amaldi U., Fisica delle radiazioni, Boringhieri Editore, 1971.

[43] Leo W.R., *Techniques for nuclear and particle physics experiments*, Sprinter Verlag 1991.

[44] J.H. Hubbell, S.M. Seltzer, "Tables of X-rays Mass Attenuation Coefficients and Mass Energy-Absorption Coefficients, from 1 keV to 20 MeV for elements Z=1 to 92 and 48 Additional Substances of Dosimetric Interest", http://physics.nist.gov/PhysRefData/XrayMassCoef, April 1996.

[45] M. Bruzzi, "Radiation effects in silicon detectors for future High Energy Physics experiments: a short overview", Proceedings of the 7th International Conference on Advanced Technology and Particle Physics, Villa Olmo (Como, Italy), 15-19 October 2001.

[46] D. Binder et al., IEEE Trans. Nucl. Sci., NS-22 (1975) 2675.
[47] A. E. Waskiewicz et al., IEEE Trans. Nucl. Sci., 33 (1986) 1710.
[48] C. Pickel et al., IEEE Trans. Nucl. Sci., 32 (1985) 4176.
[49] CMS Technical Proposal, CERN/LHCC 94-38 (1994).
[50] ATLAS Technical Proposal, CERN/LHCC 94-43 (1994).
[51] P. Riedler, "Silicon pixel and strip detectors for LHC experiments", Proceedings of the 1st Coordination Meeting of the CBM Experiment at the future GSI facility, 15-16 November 2002.
[52] S. Albergo et al., Nucl. Instr. Meth., A422, 238, 1999.
[53] "Total dose steady-state irradiation test method", ESA/SCC Basic Specification No. 22900, European Space Agency.
[54] "Ionizing radiation (total dose) test procedure", MIL-STD-883E, method 1019.4.
[55] M. Menichelli, "Total dose test for commercial-off-the-shelf components to be used in a space experiment: a survey on current technologies", Proceedings of the 7th International Conference on Advanced Technology and Particle Physics, Villa Olmo (Como, Italy), 15-19 October 2001.
[56] M. Huhtinen, P. Lecomte, D. Luckey, F. Nessi-Tedaldi, F. Pauss, "High-energy proton induced damage in $PbWO_4$ calorimeter crystals", ETHZ–IPP–PR–2004–03 November 30st, 2004.

Edito dall' ENEA
Funzione Centrale Relazioni Esterne
Unità Comunicazione
Lungotevere Thaon di Revel, 76 - 00196 Roma
www.enea.it
Stampa: Laboratorio Tecnografico ENEA - CR Frascati
Finito di stampare nel mese di settembre 2005